International Journal of Automotive Technology, Vol. 16, No. 1, pp. 27–37 (2015)
DOI 10.1007/s12239–015–0003–8

pISSN 1229–9138/ eISSN 1976–3832

DESIGN AND DEVELOPMENT OF A HEADING ANGLE CONTROLLER FOR AN UNMANNED GROUND VEHICLE

S. SAHOO[1)], S. C. SUBRAMANIAN[2)*], N. MAHALE[1)] and S. SRIVASTAVA[3)]

[1)]Centre for Artificial Intelligence and Robotics, Bangalore 560 093, India
[2)]Department of Engineering Design, Indian Institute of Technology Madras, Chennai 600 036, India
[3)]Engine Control System Group, Gas Turbine Research Establishment, Bangalore 560 093, India

(Received 2 May 2013; Revised 17 August 2013; Accepted 15 January 2014)

ABSTRACT–This paper describes the design and implementation of a controller to track the desired heading angle for an unmanned ground vehicle (UGV) considering the limits on rotation of steering wheel and steering motor rate. The well-known "bicycle model" approximation, that considers the vehicle slip angle and ground-wheel interaction, has been used. In this work, combined closed loop control for steering motor and heading angle of the vehicle has been considered for better accuracy. The challenge in designing this control system is to include the actuator dynamics as the response time to steer the front wheel is in the same order as that of the heading angle dynamics of the vehicle. Experiments have been conducted, analysis of data collected is presented and the resulting mathematical representation is explained in detail. Results from both simulation and experimental implementation are also compared. It has been found that the vehicle controller can be tuned effectively to achieve the desired heading angle changes up to twenty degrees within three seconds when the vehicle is moving at a speed of 1.4 m/sec.

KEY WORDS : Unmanned Ground Vehicle (UGV), Navigation, Path tracking, Heading control

NOMENCLATURE

m	: mass of the vehicle
I_z	: yaw moment of inertia of the vehicle
δ	: steering angle of the front wheel
r	: yaw rate of the vehicle
θ	: vehicle yaw angle measured with respect to the inertial global X-axis
v	: velocity of the vehicle
F_{yf}	: lateral tire force on the front wheel
F_{yr}	: lateral tire force on the rear wheel
l	: wheelbase
l_f	: distance of front tire from vehicle CG
l_r	: distance of rear tire from vehicle CG
C_f	: cornering stiffness of the front wheel
C_r	: cornering stiffness of the rear wheel

1. INTRODUCTION

Development of Unmanned Ground Vehicles (UGVs) has been going on for decades. An unmanned ground vehicle is one that is capable of driving itself without human control. A significant task in designing controllers for an UGV involves the design and development of path trackers. A path tracker is a system that applies appropriate steering motions to guide the vehicle along the path as described by the vehicle path planner. Several algorithms for optimal path planning have been proposed in the literature (Barraquand and Latombe, 1989) and (Koenig and Likhachev, 2002). Indeed, feasible motion planning for high speed navigation in complex environments can also be generated using a model-based trajectory generation approach (Howard *et al*., 2008). Moon and Choi (2011) developed a target path planning algorithm that can be regarded as a road-smoothing procedure.

For a typical patrol mission scenario, the path can be obtained in several ways. In principle, a path should be defined as a continuous function. In practice, however, it is discretized and described either as a series of straight line segments between interim goal waypoints or as a series of closely spaced nodes typically spaced tens to hundreds of meters apart. The mission plan consists of a Point-to-Point navigation algorithm determines the desired heading angle based on the collection of these waypoints accompanied by a radial tolerance for each. For a waypoint to have been reached, the vehicle must pass it at a distance less than or equal to the radial tolerance for that waypoint. The mismatch between the desired heading angle and the actual vehicle heading angle under the real environment needs to be minimal to achieve good path tracking. In addition, this is significantly affected by the speed of the vehicle.

**Corresponding author*. e-mail: shankarram@iitm.ac.in

Using the concept of the path curvature or look-ahead distance, there are many different types of path tracking algorithms available. Three popular algorithms are follow-the-carrot, pure pursuit and vector pursuit (Wit *et al*., 2004). The first two methods have been around for quite a while now, while vector pursuit or screw tracking, as it is also called, is relatively new. The main difference between these methods is that vector pursuit uses information about orientation at the look-ahead point, while the others do not (Heredia and Ollero, 2007).

In traditional methods such as follow-the-carrot (Yeu *et al*., 2006), the goal point is determined by defining a circle in such a way that it passes through both the goal point and the current vehicle position. The orientation error was defined to be the angle between current vehicle heading and the line drawn from the centre of the vehicle coordinate system to the goal point. In a pure pursuit method (Hellstrom *et al*., 2006), the turning radius can be replaced with the look-ahead distance to include the effect of vehicle speed and heading angle. The look-ahead distance is defined as a virtual distance from the current vehicle position to a point on the mid-path in the longitudinal direction of the vehicle. As the steering angle was calculated based on the wheelbase of the vehicle and the path curvature or the look-ahead distance to minimize the orientation error, the performance was found to be overly dependent on the look-ahead distance. The look-ahead distance changes with vehicle speed. As the vehicle speed increases, the look-ahead distance typically needs to be increased (Morales *et al*., 2009). In practice, the gain or look-ahead distance is independently tuned to be stable by conducting a wide range of experiments at various speeds. In these methods, the vehicle cuts corners and there is a tendency to oscillate close to the path (Yeu *et al*., 2006). The steering angle was also assumed to change instantaneously during transition between consecutive path curvatures.

There are also many variations of the basic pure-pursuit algorithm (Hellström and Ringdahl, 2006). A vehicle named 'Sandstorm' that went farthest in the first DARPA grand challenge used the pure pursuit algorithm for path tracking. The vehicle 'Stanley' that won the DARPA grand challenge in 2005 used an intuitive steering control law based on kinematic bicycle model. 'Boss', the autonomous vehicle that won the DARPA Urban Challenge in 2007 used a predictive control strategy (Urmson *et al*., 2008) to perform vehicle control. However, it included a kinematic model of the vehicle, a time delay and rate limits on steering in the optimization of the steering controls.

Lee and Han (2008) proposed a steering control method to construct a travel path from current position to the target position as an Arc-path or S-path considering a kinematic bicycle model. As there was no rapid change in road curvature, steering saturation and rate limits were ignored in these models while travelling on a S-path. In a similar study, a nonlinear kinematic bicycle model with kinematic constraints was used to design the lateral controller (Song, 2013). But, the effect of the mass and load are neglected.

Even if there are many literatures to analyze dynamic performance of steering system (Xu and Ahmadian, 2013), it is always difficult to identify or collect required vehicle parameters from the vehicle manufacturer for simulation.

In related work, due to the difficulty of obtaining the actual vehicle dynamic parameters and due to the variability of certain model parameters, Kodagoda *et al*., (2002) discussed the idea of fuzzy controllers for the speed and steering control of an autonomous ground vehicle. Generally, in a fuzzy controller, the gains and membership functions are tuned to yield the desired performance based on trial and error and heuristics. When it is required to implement these controllers on a different test platform, comparatively more effort is required to tune the gains of the longitudinal and lateral controllers. For high speed autonomous navigation (Talvala *et al*., 2011) both feedback and feedfoward steering controller were incorporated by using a dynamic bicycle model where the steering angle requirement varies from -5 degrees to 5 degrees.

So, to bridge a gap between planning and navigation, a realistic control strategy has been proposed in this paper using Point-to-Point navigation algorithm based on a dynamic bicycle lateral vehicle model considering the steering actuator dynamics. In this method, the required steering angle is calculated from the heading angle error. Initial tests and results without considering the steering motor actuator dynamics (i.e., the dynamics of the electric motor that actuates the steering) can be found in (Sahoo *et al.*, 2012). However, it was found that the front wheels take around a second to be steered by 10 degrees and since this time is in the same order as that of the vehicle heading dynamics response time, the steering actuator dynamics has been included in this study. The details of the system model and the controller are presented in section 2. The controller performance has been compared with experiments in section 3 and concluding remarks are presented in the last section.

2. DYNAMIC MODELING OF THE SYSTEM

A simple approximation of the lateral dynamics of land vehicles is the "bicycle model". This approximation combines the effects of the two front wheels and treats them as a single wheel. The bicycle model also combines the two rear wheels and treats them as a single wheel.

2.1. Linearized Dynamic Bicycle Model

A linearized model, often sufficient to provide satisfactory performance in the operating range of interest, is widely used in control system design. In most land vehicle control applications, a linear and time invariant (LTI) model is used. A bicycle model of the vehicle with two degrees of freedom, as shown in Figure 1, is considered in this study. The two degrees of freedom are represented by the vehicle lateral position, y, and the vehicle yaw angle, θ.

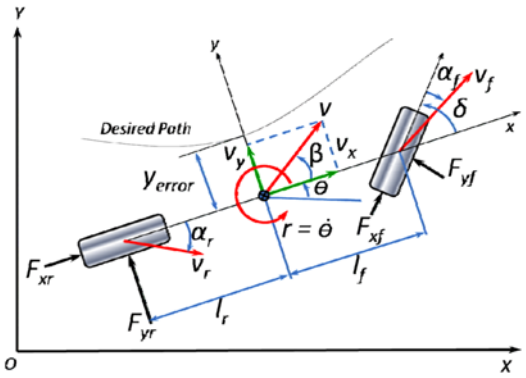

Figure 1. Dynamic bicycle model.

The vehicle lateral position is measured along the lateral axis of the vehicle and the vehicle yaw angle is measured with respect to the global *X*-axis. The lateral force at the tire-road interface depends on the slip angle. Figure 1 illustrates the bicycle model for a vehicle with no roll motion. It is assumed that only the front wheel is steerable.

The lateral motion of the vehicle is described by

$$m\dot{v}_y = F_{xf}\sin\delta + F_{yf}\cos\delta + F_{yr}. \tag{1}$$

The equation governing the yaw motion is

$$I_z\dot{r} = l_f F_{xf}\sin\delta + l_f F_{yf}\cos\delta - l_r F_{yr}. \tag{2}$$

Considering δ to be small, (1) and (2) can be written as

$$m\dot{v}_y = F_{yf} + F_{yr} \text{ and } I_z\dot{r} = l_f F_{yf} - l_r F_{yr}. \tag{3}$$

The acceleration vector is written as

$$\mathbf{a} = (\dot{v}_x - v_y r)\mathbf{i} + (\dot{v}_y + v_x r)\mathbf{j}, \tag{4}$$

where **i** and **j** are the unit vectors in x and y directions respectively. Here, v_x and v_y are the velocity components in the x and y directions respectively. The x–y coordinate system is fixed to the vehicle. Substituting the y-component of the acceleration from (4) into (3), the lateral motion of the vehicle is described by

$$m(\dot{v}_y + v_x r) = F_{yf} + F_{yr}. \tag{5}$$

Experimental results show that the lateral tire force of a tire is proportional to the slip-angle for small slip-angles (Ray, 2009). The slip angle of a tire is defined as the angle between the orientation of the tire and the direction of the velocity vector at the tire. For small slip angles, the lateral forces acting on the front and rear wheels can be written as

$$F_{yf} = C_f\,\alpha_f \text{ and } F_{yr} = C_r\,\alpha_r. \tag{6}$$

The slip angles of the front and rear wheels are

$$\alpha_f = \delta - \left(\frac{v_y + l_f r}{v_x}\right) \text{ and } \alpha_r = -\left(\frac{v_y - l_r r}{v_x}\right). \tag{7}$$

Using (6) and (7), the governing equation (3) becomes

$$m\dot{v}_y + \left(\frac{C_f + C_r}{v_x}\right)v_y + \left(mv_x + \frac{C_f l_f - C_r l_r}{v_x}\right)r = C_f\,\delta \tag{8}$$

$$I_z\dot{r} + \left(\frac{C_f l_f - C_r l_r}{v_x}\right)v_y + \left(\frac{C_f l_f^2 + C_r l_r^2}{v_x}\right)r = C_f l_f\,\delta. \tag{9}$$

The transfer function, $G_\delta^r(s)$ that relates the response of the yaw rate to the steering angle, is obtained as

$$G_\delta^r(s) = \frac{a_{r1}s + a_{r2}}{s^2 + 2\xi\omega_n s + \omega_n^2}, \tag{10}$$

where $a_{r1} = \dfrac{C_f l_f}{I_z}$, $a_{r2} = \dfrac{C_f C_r l}{mI_z v_x}$,

$$2\xi\omega_n = \frac{m(C_f l_f^2 + C_r l_r^2) + I_z(C_f + C_r)}{mI_z v_x},$$

and $\omega_n^2 = \dfrac{C_f C_r l^2}{mI_z v_x^2} - \dfrac{(C_f l_f - C_r l_r)}{I_z}$.

The transfer function, $G_s^\theta(s)$ that relates the response of the heading angle to the steering angle, is obtained as

$$G_s^\theta(s) = \frac{a_{r1}s + a_{r2}}{s(s^2 + 2\xi\omega_n s + \omega_n^2)}. \tag{11}$$

2.2. Modeling the Steering Actuator

In order to maintain the vehicle heading angle, the steering wheels of the UGV should follow the command signals received from the vehicle controller and maintain synchronization with the steering actuator. To perform the simulation of the system, an appropriate actuator model needs to be established. Therefore, the transfer function model is derived analytically from the electrical and mechanical governing equations of the motor that is obtained from first principles. To model the steering actuator, a visualization as shown in Figure 2, is considered.

The steering motor torque T is related to the armature current i, by a torque constant K_t. The governing equations based on the Newton's law combined with the Kirchoff's law are

$$J\frac{d^2\phi}{dt^2} + b\frac{d\phi}{dt} = K_t i, \tag{12}$$

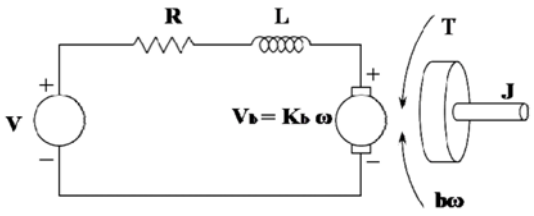

Figure 2. Schematic diagram of the steering actuator system.

and $L\frac{di}{dt}+Ri=V-K_b\frac{d\phi}{dt}$. (13)

where φ is the angle of rotation of the steering motor shaft, J is the rotor inertia and b is the viscous-friction coefficient of the combination of the motor, load, and gear train. Applying the Laplace transform to (12) and (13), the transfer function, $G_V^{\phi}(s)$ that relates the response of the angle of rotation of the steering motor shaft, $\varphi(s)$, to the input voltage, $V(s)$, is obtained as

$$G_V^{\phi}(s)=\frac{1}{s}\left(\frac{K_t}{(Ls+R)(Js+b)K_t+K_b}\right). \quad (14)$$

2.3. Closed-Loop Feedback for Desired Heading Angle

Let us consider a closed-loop negative feedback system for tracking the desired heading angle as shown in Figure 3. The output of this model is the heading angle while the input is the steering angle that is measured by an incremental encoder attached to the steering motor. The time taken for steering the front wheel by 10 degrees is around one second and since this is in the same order as the response time of the vehicle heading dynamics, the model of the steering motor system has been included in this study.

The controller designed for this system has been decoupled into 2 loops. The inner loop controller, H_V^{ϕ}, controls the error between the desired and current rotation of the steering motor and the input of this loop is a function of the steering angle that is calculated based on the error in the heading angle of the vehicle. The outer loop controller, H_{θ}^{δ}, diminishes the error between the desired and actual heading angles of the vehicle.

2.4. Test Platform

In order to implement and verify the proposed control strategies, a commercially available 4-wheeled battery operated vehicle was modified to fulfill the experimental requirements. The test platform after modification and mounting of equipment is shown in Figure 4.

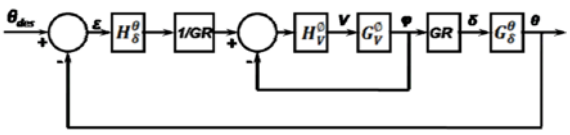

Figure 3. Negative feedback system for desired heading angle.

Figure 4. Test platform.

A DC motor with a controller is used to accelerate and decelerate the vehicle in the longitudinal direction. The paddle position is sent to the motor driver to control the speed of the vehicle. The electric power is supplied from 48V batteries that could drive the vehicle with a maximum speed of 30 km/hr. The steering system is a self adjusting rack and pinion steering. The conventional steering system was modified for automated operating by installing another DC motor (Maxon RE-40) with a 156:1 reduction gear ratio at the steering shaft. This motor is connected to the steering shaft with the help of spur gears. The rotation of the steering shaft can be measured by the encoder attached to the steering motor. The front body of the vehicle is modified to provide the space for mounting the sensors.

The primary means of localization is by a Global Positioning System (GPS). To cater for likely eventualities such as GPS inaccuracy, outage or denial, the system also has an accurate Inertial Navigation System (INS) onboard, which will augment and be augmented by the GPS. The INS comprises an odometer, a compass and the Inertial Measurement Unit (IMU).

2.5. Model Parameter Identification

The dynamic bicycle model has parameters that are not directly measureable. However, a workable estimate can be obtained using commonly available tools. So, the total mass the vehicle, the C.G. location and the moment of inertia were estimated by measuring the vehicle's split mass, utilizing four measuring scales under each wheel. The total mass of the vehicle is the sum of the measurements of mass under each wheel and is estimated as

$$m=m_{fl}+m_{fr}+m_{rl}+m_{rr}, \quad (15)$$

where m_{fl}, m_{fr}, m_{rl}, and m_{rr} are the mass of the vehicle at front-left, front-right, rear-left and rear-right respectively. Both the front and rear wheels are considered as a single wheel at the center of the corresponding axle. The front wheel mass, m_f, and the rear wheel mass, m_r, are given by $m_f=m_{fl}+m_{fr}$ and $m_r=m_{rl}+m_{rr}$.

From this and a measurement of the wheel base l, the location of the vehicle's C.G., described by distances l_f and l_r from the front and rear axles along the center line is obtained as

$$l_f=l\left(1-\frac{m_f}{m}\right) \text{ and } l_r=l\left(1-\frac{m_r}{m}\right).$$

The vehicle's moment of inertia is approximated by treating the vehicle as two point masses joined by a mass-less rod. The moment of inertia for the vehicle is given by

$$I_z=m_f\,l_f^2+m_r\,l_r^2. \quad (16)$$

Finally, the cornering stiffness parameters C_f and C_r must

Table 1. Parameters of the test vehicle.

Parameter	Value	Unit
l	1.93	m
w	0.90	m
l_f	1.31	m
l_r	0.62	m
m_{fl}	158	kg
m_{fr}	137	kg
m_{rl}	360	kg
m_{rr}	269	kg
I_z	932.4	kg.m^2
C_f	27359	N/rad
C_r	58335	N/rad

Table 2. Parameters of the Maxon (RE-40) DC Motor.

Parameter	Value	Unit
Terminal resistance (R)	0.317	ohms
Terminal inductance (L)	0.0823	mH
Torque constant (K_t)	30.2	mNm/A
Speed constant	317 (33.196)	rpm/V (rad/sec / V)
Back emf constant (K_b)	0.0301	V/rad /sec
Rotor inertia (J)	138	g.cm^2
Speed / torque gradient	3.33	rpm / mNm
Nominal speed (N)	6930	rpm
Nominal torque (T) (max. Continuous torque)	170	mNm
Nominal voltage	24	V

be identified. These parameters can be obtained from data sheets provided for the specific tire. As cornering stiffness parameters C_f and C_r are not readily available for this vehicle, it is normalized by the vertical load. At one degree of slip angle, the average bias tire will produce a lateral force of 10% of the vertical load. On average, radial tires have a higher cornering stiffness than bias-ply-tires. For radial tires, it is considered that cornering stiffness per degree of slip angle is approximately 16–17% of the load on the tire (Gillespie, 1992). Thus,

$$\begin{aligned} C_f &= m_f * g * 0.165 (N/\text{deg}) \\ C_r &= m_r * g * 0.165 (N/\text{deg}) \end{aligned}. \tag{17}$$

The specification data for the test vehicle considered in this study are listed in Table 1 (Sahoo *et al*., 2012).

3. IMPLEMENTATION AND EXPERIMENTAL RESULTS

The control system has been tested for tracking different step inputs of desired heading angles with a maximum overshoot of 10% and a settling time less than 5 sec. The longitudinal velocity of the vehicle has been kept constant at 1.4 m/sec. The control gains that would place the closed loop poles in the desired locations (corresponding to the above performance specifications) have been analytically determined and subsequently used in the experimental implementation. Substituting the values of the vehicle parameters from Table 1 in (11), the transfer function, is obtained as

$$G_\delta^\theta(s) = \frac{38.44(s+66.24)}{s(s+53.15)(s+66.24)}. \tag{18}$$

The common pole-zero pair at –66.24 occurs because the cornering stiffness of the front and rear tires are calculated based on the percentage of the vertical load on each tire. However, the common pole-zero pair can be cancelled here as it occurs in the left half of the s-plane. Thus, (18) can be written as

$$G_\delta^\theta(s) = \frac{38.44}{s(s+53.15)}. \tag{19}$$

3.1. Design of Steering Controller

A DC motor (Maxon RE-40) with a 156:1 reduction gear ratio is installed at the steering rod for controlling the heading direction. The steering motor is connected to the steering shaft with the help of spur gears with a gear reduction ratio of 1.47. One rotation of the steering shaft requires $156*1.47 \approx 230$ number of rotations of the steering motor. The standard rack and pinion steering system of the vehicle has a gear ratio of 15.5. So, the gearing ratio between the front wheel and the steering motor is $156*1.47*15.5 \approx 3555$. The specification data for the Maxon RE-40 DC motor are listed in Table 2.

The steering motor steers the front wheels of the vehicle based on the command signals received from the controller. So, it is necessary to determine the required steering angle to follow the desired heading angle. This means that the steering wheel angle should track the steering motor angle. Therefore, the steering wheel control system should have a quick response, suitable damping, and minimal tracking error. Based on these requirements, a negative servo feedback control structure is implemented for the steering wheel control system. As a result, the tracking requirement for the steering wheel becomes a design problem for the steering motor servo control system. At steady state, the angular velocity of the motor, $\omega = d\varphi/dt$ is constant. So, the governing equation (12) becomes

$$b\omega = T, \tag{20}$$

where the motor torque T is related to the armature current i, by a torque constant K_t. Therefore, for a nominal motor

speed of 6930 rpm (≈ 725 rad/sec) and nominal torque of 0.170 Nm, the viscous-friction coefficient b, is calculated as 2.34e-5 Nm.rad/sec. As the gearing ratio is quite high, the moment of inertia of the combination of the motor, load, and gear train is considered as equal to the moment of inertia of the motor. The terminal inductance, L, of the motor is 0.0823 mH and the rotor inertia J is 138 g.cm^2. So, the coefficient of s^3 in the denominator of (14) is found to be 1.14e-9 H.kg.m^2. Hence, the term JLs^3 in the in the denominator of (14) can be neglected. Substituting the values of the motor parameters from Table 1 in (14), the transfer function for angle of rotation to input voltage, $G_V^{\phi}(s)$ is obtained as

$$G_V^{\phi}(s) = \frac{1}{s}\left(\frac{302}{0.044s + 9.164}\right). \tag{21}$$

A proportional controller was used to control the steering motor that will rotate the front wheels of the vehicle judiciously to achieve the desired heading angle. The desired angle of the front wheel steering angle is converted to an angle of the rotation of the steering motor. The steering controller will adjust the input voltage to achieve the desired angle by calculating the error. The rotation of the motor shaft can be measured by the encoder attached to the steering motor. This angle will be fed back to the steering controller. In order to achieve smooth high-speed motion without over-taxing the motor, the controller must direct the motor driver to change velocity judiciously to achieve optimum results. This is accomplished using shaped velocity profiles to limit the accelerations and decelerations required. Data were collected for the steering wheel's response to various commanded step inputs. Again, with this data, the saturation points of the steering wheel's velocity and acceleration were determined experimentally. From the experiment, it has been found that the proportional steering controller, $H_V^{\phi} = 2$ gives better result as the maximum error is within 5% when compared with the simulated result.

The steering angle tracking response has been simulated using MATLAB-Simulink. However, for the purpose of simulation, a saturation block has been added to restrict the voltage input from -20 to +20 Volts. The input to the system is a step input of the desired steering angle. A wide range of experiments were conducted and these results are compared with the simulation results. As shown in Figure 5, the slope of the response of the steering wheel is found to be approximately 10 degrees per second.

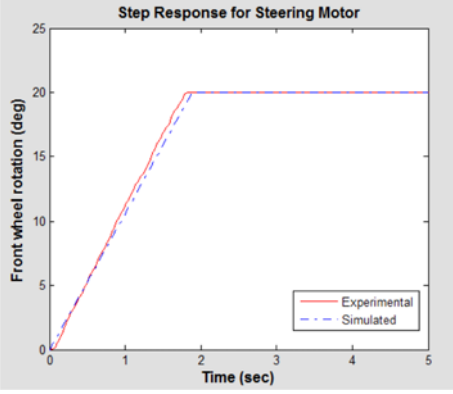

Figure 5. Response of front wheel to step input of 20 degrees.

3.2. Combined Steering and Heading Control

Considering the steering controller, $H_V^{\phi} = 2$, from (21) the closed loop transfer function for the angle of rotation to the input voltage of the steering motor, $G_m(s)$, is obtained as

$$G_m(s) = \frac{604}{0.44s^2 + 9.164s + 604}. \tag{22}$$

As shown in Figure 3, combining the closed loop steering motor transfer function from (22) and the vehicle heading transfer function from (19), the overall system transfer function can be obtained as

$$G(s) = \frac{23218}{0.044s^4 + 11.5s^3 + 1091s^2 + 32097s}. \tag{23}$$

3.2.1. Proportional controller

Consider a proportional heading angle controller,

$$H_{\theta}^{\delta}(s) = K_P. \tag{24}$$

The maximum overshoot requirement of 10% of steady state response results in the damping ratio, ζ, being less than 0.6. The characteristic equation for this negative closed loop feedback system is

$$0.044s^4 + 11s^3 + 1091s^2 + 32097s + 32097\,K_P = 0.$$

For a better understanding of the system behavior and to reduce the settling time, the heading angle tracking response without considering actuator dynamics has been simulated using MATLAB-Simulink and also compared with considering actuator dynamics. For the proportional controller, the value of K_P that satisfies the performance requirements was found to be 1.3.

Several experiments have been carried out to check the theoretical results explained in the preceding sections. These tests have been carried out on the test platform (shown in Figure 4). In each test performed, the vehicle was commanded to move in a straight line for 5 seconds to achieve a constant forward velocity of 1.4 m/sec and then it commanded to achieve a desired change in heading angles of 20 degrees. Experimental and simulated results for the heading angle response and steering angle response are shown in Figure 6 and Figure 7 respectively.

Considering the steering actuator dynamics in simulation, the settling time is found to be 4 seconds for K_p = 1.3. For the same K_p value, experimental result shows that the desired heading angle can be achieved in 2.9 seconds and

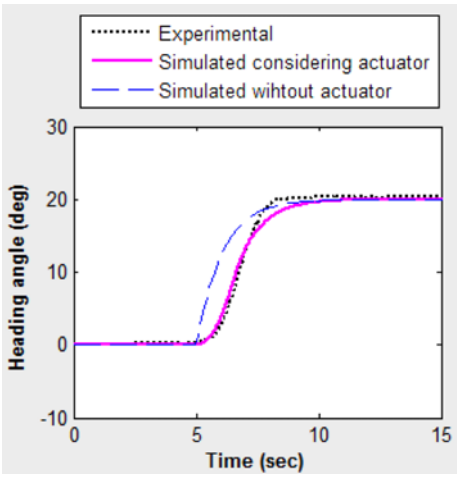

Figure 6. Comparison of experimental and simulated heading angle responses for a desired heading angle of 20 degrees with proportional controller for K_p = 1.3.

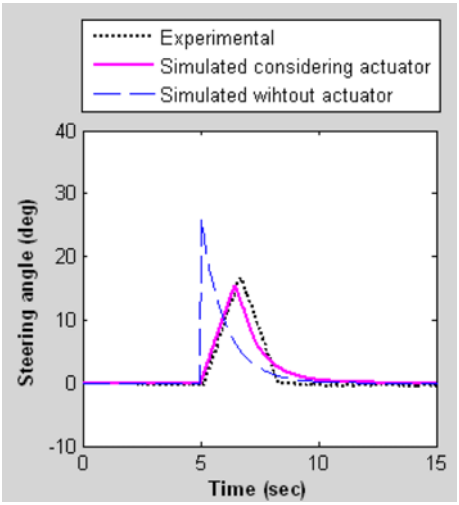

Figure 7. Comparison of experimental and simulated results of steering angle response for desired heading angle of 20 degrees with K_p = 1.3.

the steering angle requirement has gone up to 16.7 degrees. There is no overshoot and the steady state error is within the 5% limit. Considering the actuator dynamics in simulation, the steering angle requirement is 15.6 degrees.

It can be observed from Figure 6 that the maximum error in the heading angle between the experimental and simulated results is 9.1 degrees and 2.1 degrees without actuator dynamics and with actuator dynamics respectively. So, the simulated heading angle is in good agreement with the experimentally measured heading angle when the steering actuator dynamics is included in the system model. This shows that the incorporation of the actuator dynamics is important in this particular study. It can be observed from Figure 7 that the steering angle required by the controller is practically unrealizable when the actuator dynamics is not incorporated.

3.2.2. Proportional and Integral (PI) controller

Consider a PI heading angle controller,

$$H_\theta^\delta(s) = K_P + \frac{K_I}{s} = \frac{K_P(s+Z_0)}{s}. \quad (25)$$

where $Z_0 = K_I / K_P$. As (25) shows, the controller adds a pole at the origin as well as a zero at $-Z_0$, which is influenced by the choice of K_I and K_P. Integral control bases its corrective action on the cumulative error integrated over time and is used to eliminate the steady state errors.

For the PI controller, simulation has been carried out in MATLAB using control and estimation tools manager. It is found that K_P =1.6 and K_I = 0.48 do not able to meet the performance requirements, but it tunes the model better. Experimental and simulated results for the heading angle response and steering angle response are shown in Figure 8 and Figure 9 respectively.

Using this PI controller considering the actuator dynamics in simulation, the settling time is found to be 7 seconds. Though the steady state error has been eliminated, the overshoot has gone beyond 50%. From the experimental result, it has been found that for K_P =1.6 and K_I = 0.48, the desired heading angle can be achieved in 5.5 seconds and the steering angle requirement has gone up to 19.5 degrees. Though the steady state error has been eliminated, the overshoot has gone up to 35% which is the beyond the acceptable limits.

The maximum error in the heading angle between the experimental and simulated results is 13.2 degrees and 4.9 degrees without actuator dynamics and with actuator

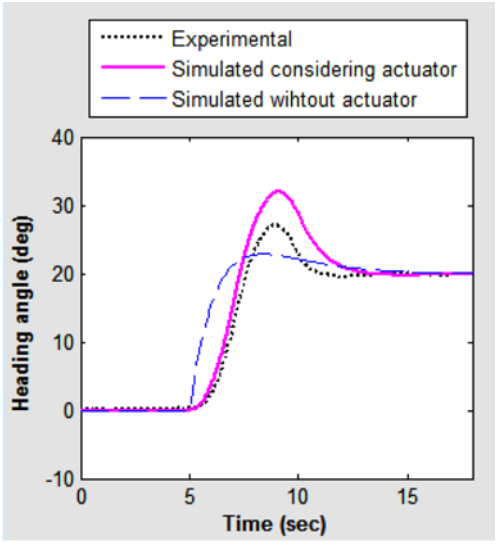

Figure 8. Comparison of experimental and simulated heading angle responses for a desired heading angle of 20 degrees with PI controller for K_P =1.6 and K_I = 0.48.

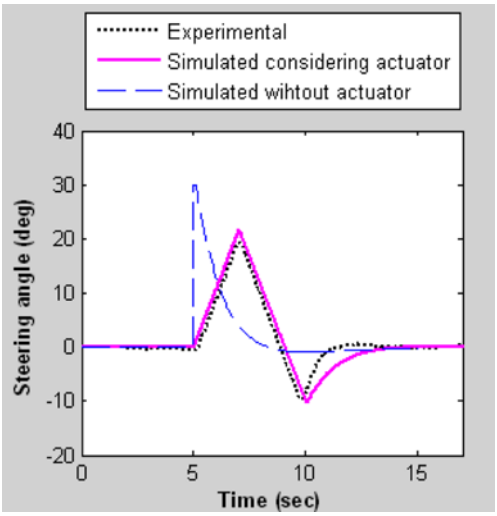

Figure 9. Comparison of experimental and simulated results of steering angle response for desired heading angle of 20 degrees with K_P =1.6 and K_I = 0.48.

dynamics respectively. It has also been found that without considering actuator dynamics, there is a sudden rise in steering angle requirement that is impractical. Considering the actuator dynamics the simulation result is in good agreement with the experimental result. However, the difference may be due to the nonlinearity nature of the front wheel steering as it requires 2 to 3 times more torque after it reaches 20 degrees towards the extreme left or right side of the vehicle. When the steering angle requirement goes beyond 20 degrees, the small angle approximation does not hold good. In addition to that, it may be due to the shifting of the vehicle CG towards the left as the load in the left side of the vehicle is more than the right of the load.

3.2.3. Proportional and Derivative (PD) controller

Consider a PD heading angle controller

$$H_\theta^\delta(s) = K_p + K_d\, s = K_p(1 + Z_0 s)\,, \tag{26}$$

where $Z_0 = K_d / K_p$. As (26) shows, the controller adds a zero at $-Z_0$, which is influenced by the choice of K_p. In order to satisfy the performance requirements, it was determined that $-Z_0$ should be close to the origin. Therefore, the derivative gain should be small compared to the proportional gain.

For the PD controller, the simulation has been carried out in MATLAB. Considering the same K_p = 1.8, it has been found that K_d = 0.4 satisfies the performance requirements. To compare the simulation result with the experimental results, several tests have been carried out for different heading angles keeping K_d = 0.4. In each of the tests performed, the vehicle was commanded to achieve a constant forward velocity of 1.4 m/sec and then follow different heading angles. For the PD controller with K_p = 1.8 and K_d = 0.4, experimental result shows that the settling time was found to be 3 seconds with no overshoot. As shown in Figure 10, the steady state error is within the limit of 5% error and the steering requirement has gone up to 16.3 degrees.

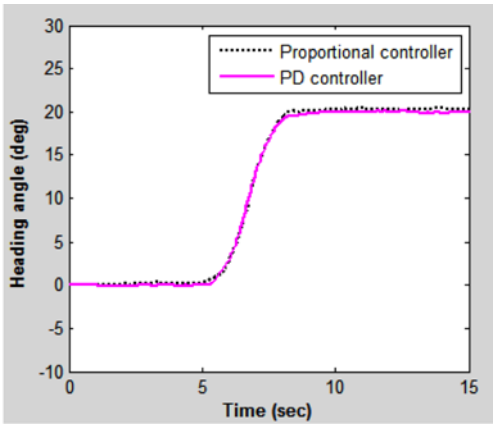

Figure 10. Comparison heading angle responses for proportional and PD controllers to achieve a desired heading angle of 20 degrees.

It is obvious from Figure 10 that the performance of the PD controller (K_p = 1.8 and K_d = 0.4) is comparable with the proportional controller (K_p = 1.3). As both experimental and simulated performance of PD controller is very close to the proportional controller, it makes more sense to make a comparison between the experimental results of PD controller and proportional controller. So, comparison between the experimental and simulation results for PD controller are not presented here. Based on the experimental data, a comparison between the steering response for the PD controller and the proportional controller is shown in Figure 11.

However, from the simulation, it has been found that for the PD controller keeping K_d = 0.4, increasing the value of K_p beyond 1.8 reduces the settling time. But, implementing this on the test platform to achieve the desired heading angle, the steering angles start oscillating. Since the

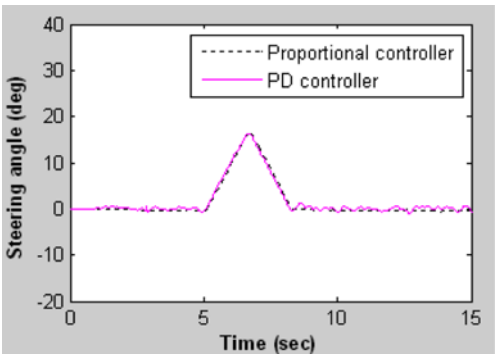

Figure 11. Comparison of experimental results of steering angle response for proportional and PD controllers.

inherent damping due to the tire forces decreases near saturation, the yaw dynamics become more oscillatory at the limits of handling. Yaw oscillation is undesirable and creates unnecessary tire slip. It also reduces the available tire force that can be used for accelerating the vehicle along the path. So the K_p value for the PD controller is considered as 1.8.

As shown in Figure 10, both the proportional and PD controller meets the performance requirements. However, in comparison to the proportional controller, the steady state error in PD controller is 0.5% lesser. The steering angle requirement of PD controller is 16.3 degrees, where as in case of proportional controller, it is 16.7 degrees. However, the settling time for the PD controller is 0.1 seconds slower than the proportional controller.

3.2.4. Tracking of a mission plan

For a typical patrol scenario, using the Point-to-Point algorithm, the mission plan is generated by a set collected waypoints that are received from the GPS. The path to be tracked is the straight line segment between the previous waypoint and the next waypoint. Based on the collection of these waypoints, the navigation algorithm determines the desired heading angle with an increment of 20 degrees from its current heading angle. To keep the vehicle moving along the path, the vehicle has to maintain its heading close to the desired heading angle. The heading angle towards left side of the vehicle when seen from the back is considered as positive and towards right is negative. Initially, the vehicle was commanded to move in a straight line for 5 seconds to achieve a constant forward velocity of 1.4 m/sec. The result in Figure 12 shows that considering a realistic control strategy based on a dynamic bicycle lateral vehicle model and using the PD controller (K_p = 1.8 and K_d = 0.4), the actual heading angle tracks the desired heading angle in a smooth manner and the vehicle closely follows the predefined trajectory. However, it can be improved by considering lateral distance error. The experimental steering angle response of the vehicle to achieve the mission plan is shown in Figure 13.

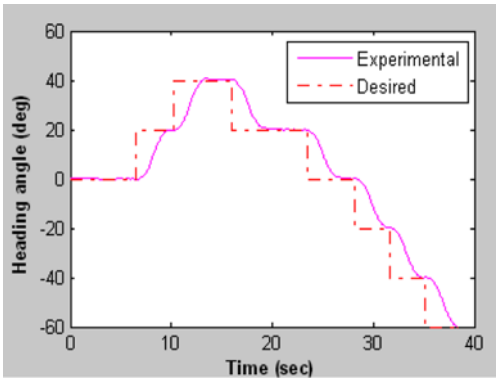

Figure 12. Comparison of experimental and desired heading angle response with PD controller to achieve the mission plan.

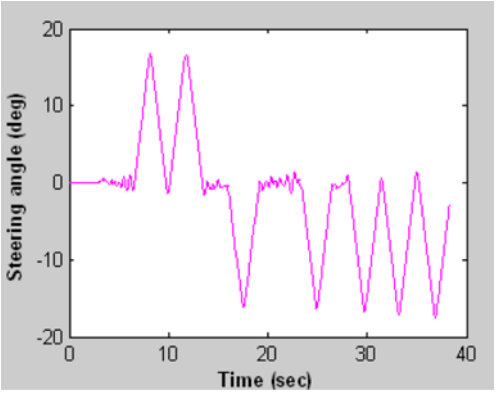

Figure 13. Experimental steering angle response of the vehicle with PD controller to achieve the mission plan.

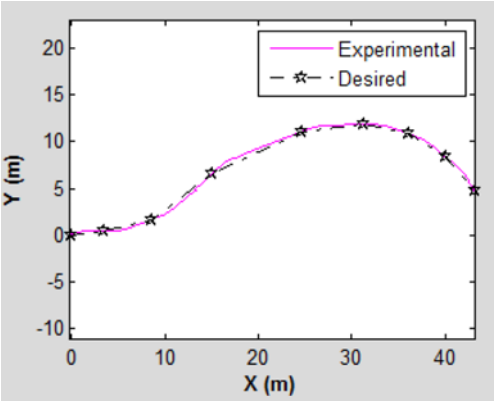

Figure 14. Comparison of experimental bird's eye view with the desired mission plan using a PD controller.

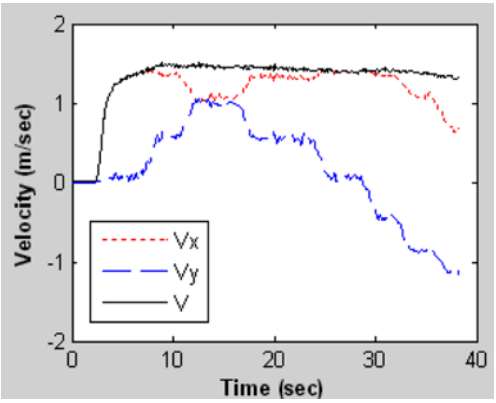

Figure 15. Experimental longitudinal, lateral and resultant velocity response of the vehicle with PD controller to achieve the mission plan.

The experimental bird's eye view is compared with the desired mission plan in Figure 14. To achieve a smooth transition when the desired heading angle changes,

trajectory planning has to be included rather commanding an step input of 20 degrees. The experimental longitudinal, lateral and resultant velocity response of the vehicle are shown in Figure 15.

4. CONCLUSION

This work has presented the analysis, design, tuning, and implementation of different path tracking controllers using the Point-to-Point navigation algorithm considering the dynamic bicycle model for path tracking of an autonomous ground vehicle equipped with IMU and GPS. Moreover, the influence of design parameters has also been studied experimentally. The controller designed for this system has been decoupled into two loops. The inner loop controller, controls the error between the desired and current rotation of the steering motor and the input of this loop is a function of the steering angle that is calculated based on the error in the heading angle of the vehicle. The outer loop controller, diminishes the error between the desired and actual heading angles of the vehicle. The time taken for steering the front wheel to reach 10 degrees is around one second and since this is in the same order as the response time of the vehicle heading dynamics, the model of the steering actuator dynamics has been included in this study.

The simulated and the experimental results demonstrated that the proposed PD controller regulated the steering motor to follow the desired heading angle in a reliable and smooth way in an outdoor environment. When the vehicle is moving at a constant velocity of 1.4 m/sec, a heading angle change up to 20 degrees can be achieved within 3 seconds with less than 2% steady state error. Extensive simulation and experimental results show that this control strategy performs well at low speeds and the vehicle can be navigated closely to the path to be followed. Any patrol mission specified as a sequence of waypoints could be tracked using these control strategies. Although this analysis was performed on a smaller battery operated vehicle, the proposed methodology can be applied to other autonomous vehicles.

For future work, the system model can be used to integrate the lateral control and longitudinal control. It can also be used to estimate unknown parameters such as the cornering stiffness of tires.

ACKNOWLEDGEMENT–The authors thank the Director, CAIR, for granting permission to publish the results of this research.

REFERENCES

Barraquand, J. and Latombe, J. C. (1989). On nonholonomic mobile robots and optimal maneuvering. *Proc. IEEE Int. Symp. Intelligent Control*, 340–347.

Gillespie, T. D. (1992). *Fundamentals of Vehicle Dynamics*. Society of Automotive Engineers. Warrendale. 347–355.

Hellstrom, T., Johansson, T. and Ringdahl, O. (2006). *Development of an Autonomous Forest Machine for Path Tracking*. Field and Service Robotics. Springer. New York. 603–614.

Hellström, T. and Ringdahl, O. (2006). Follow the Past: A path-tracking algorithm for autonomous vehicles. *Int. J. Vehicle Autonomous Systems* **4**, **2/4**, 216–224.

Heredia, G. and Ollero, A. (2007). Stability of autonomous vehicle path tracking with pure delays in the control loop. *Advanced Robotics* **21**, **1/2**, 23–50.

Howard, T. M., Green, C. J. and Kelly, A. (2008). State space sampling of feasible motions for high-performance mobile robot navigation in complex environments. *J. Field Robotics* **25**, **6/7**, 325–345.

Koenig, S. and Likhachev, M. (2002). Improved fast replanning for robot navigation in unknown terrain. *Proc. IEEE Int. Conf. Robotics and Automation (ICRA)*, 968–975.

Kodagoda, K. R. S., Wijesoma, W. S. and Teoh, E. K. (2002). Fuzzy speed and steering control of an AGV. *IEEE Trans. Control Systems Technology* **10**, **1**, 112–120.

Lee, K. B. and Han, M. H. (2008). Lane-following method for high speed autonomous vehicles. *Int. J. Automotive Technology* **9**, **5**, 607–613.

Morales, J., Martinez, J. L., Martinez, M. A. and Mandow, A. (2009). Pure-Pursuit reactive path tracking for nonholonomic mobile robots with a 2D laser scanner. *EURASIP J. Advances in Signal Processing*, Article ID 935237.

Moon, C. and Choi, S. B. (2011). A driver model for vehicle lateral dynamics. *Int. J. Vehicle Design* **56**, **1/2/3/4**, 49–80.

Ray, L. E. (2009). Estimation of terrain forces and parameters for rigid-wheeled vehicles. *IEEE Trans. Robotics* **25**, **3**, 717–726.

Sahoo, S., Subramanian, S. C. and Srivastava, S. (2012). Design and implementation of a controller for navigating an autonomous ground vehicle. *Proc. IEEE Int. Conf. Power, Control and Embedded Systems (ICPCES)*, 247–252.

Song, B. (2013). Cooperative lateral vehicle control for autonomous valet parking. *Int. J. Automotive Technology* **14**, **4**, 633–640.

Talvala, K. L. R., Kritayakirana, K. and Gerdes, J. C. (2011). Pushing the limits: From lane keeping to autonomous racing. *Annual Reviews in Control*, **35**, 137–148.

Urmson, C., Anhalt, J., Bagnell, D., Baker, C., Bittner, R., Clark, M. N., Dolan, J., Duggins, D., Galatali, T., Geyer, C., Gittleman, M., Harbaugh, S., Hebert, M., Howard, T. M., Kolski, S., Kelly, A., Likhachev, M., Mcnaughton, M., Miller, N., Peterson, K., Pilnick, B., Rajkumar, R., Rybski, P., Salesky, B., Seo, Y. W., Singh, S., Snider, J., Stentz, A., Whittaker, W., Wolkowicki, Z., Ziglar, J., Bae, H., Brown, T., Demitrish, D., Litkouhi, B.,

Nickolaou, J., Sadekar, V., Zhang, W., Struble, J., Taylor, M., Darms, M. and Ferguson, D. (2008). Autonomous driving in urban environments: Boss and the urban challenge. *J. Field Robotics* **25**, **8**, 425–466.

Wit, J., Crane, C. D. and Armstrong, D. (2004). Autonomous ground vehicle path tracking. *J. Robotic Systems* **21**, **8**, 439–449.

Xu, Y. H. and Ahmadian, M. (2013). Study on the performance of active front steering system. *Int. J. Automotive Technology* **14**, **4**, 595–603.

Yeu, T. K., Park, S. J., Hong, S., Kim, H. W. and Choi, J. S. (2006). Path tracking using vector pursuit algorithm for tracked vehicles driving on the soft cohesive soil. *SICE-ICASE Int. Joint Conf*. Bexco, Busan, Korea. 2781–2786.